Thermal conduction in clumpy discs and BLR clouds

Hussein Ayad, Maryam Samadi and Shahram Abbassi[*]

Department of Physics, Faculty of Science, Ferdowsi University of Mashhad, Mashhad, 91775-1436, Iran

ABSTRACT

We investigate the dynamics of clumps that coexisted with/in advection-dominated accretion flows (ADAFs) by considering thermal conductivity. Thermal conduction can be one of the effective factors in the energy transportation of ADAFs; hence it may indirectly affect the dynamics of clumps by means of a contact force between them and their host medium. We first study the ensemble of clumps by assuming them as collisionless particles, and secondly we find the orbital motion of these clouds as individuals. For both parts, clumps are subject to the gravity of the central object and a drag force. The strong coupling between clumps and ADAF leads to equality between the average treatment of the clumps and the dynamics of their background. By employing the collisionless Boltzmann equation, we calculate the velocity dispersion of the clumps, which turns out to be approximately one order of magnitude higher than the ADAF. In fact, involving drag force in such a system causes the angular momentum of the clumps to be transported outwards by the ADAF, and hence the clouds eventually will be captured at the tidal radius. The results show that the presence of thermal conduction increases the root of the averaged radial velocity square, and this, in turn, speeds up the process of capturing the clouds through the tidal force. In the end, we focus on a typical individual cloud; the spiral orbits appear only due to the toroidal component of friction force. The parametric study again proves that the operation of thermal conduction helps in decreasing the lifetime of clumps.

Key words: accretion, accretion disc – conduction – methods: analytical.

1 INTRODUCTION

Nowadays, we have a lot of valuable information at different wavelengths, which enable us to study visible celestial objects like planets, stars, and galaxies as long as some non-visible active astronomical objects such as black holes and neutron stars exist. It is widely believed that the main engine of these invisible objects is the accretion process. In fact, accretion discs include a wide range of scales: millions of kms in low-mass X-ray binaries and cataclysmic variables, solar radius-to-au scale discs in protostellar objects, and au-to-parsec scale discs in active galactic nuclei (AGN; Spruit 2010).

Since 1952, the simplest model for accreting systems with spherical symmetry was proposed by Bondi, and several models of accretion have been introduced to describe the basic features of emergent spectrum arising from the rotating medium around compact objects. The main types of black hole accretion flows are classified based on their apparent shapes and the transportation mechanism of viscously dissipated energy (Frank, King & Raine 1992; Narayan, Mahadevan & Quataert 1998; Yuan & Narayan 2014). In the earliest class, the flow forms a geometrically thin (but optically thick) disc with relatively low temperature and the internal pressure support is small (e.g. Frank et al. 1992). In the standard thin disc model, ions and electrons have equal temperatures ($T_i = T_e$), and also the heating and cooling rates are balanced ($Q^- = Q^+$). In the second class, flow is specified with two temperatures, one for ions and an equal or smaller one for electrons. These flows are thermally unstable although both rates of cooling and heating are equal (Piran 1978; cf. Rees et al.

1982). The third class is a slim disc or optically thick hot accretion flow that occurs when the cooling rate becomes less than the heating rate ($Q^- < Q^+$), and ion temperature becomes equal to electron temperature ($T_i = T_e$). The other important class is advection-dominated accretion flow (ADAF), which is mainly optically thin. Like the second class, the ions' temperature differs from the electrons in this solution. The main factor of this type, which remarks it, is the photon trapping and carrying viscously dissipated energy towards the disc's centre. This inner movement of energy makes the flow stable (Narayan & Yi 1995). Finally, the model of luminous hot accretion flow is another solution (proposed by Yuan 2003) that the cooling process provides by radiation and decrease of entropy.

In all models mentioned above, the fluid is assumed to be continuous and homogeneous, but this is just valid in the limit of low-mass accretion rates. In luminous hot accretion flows and slim discs, the mass accretion rate is large, even larger than the critical value, so it causes thermal instability and leads to the form of cold dense clumps, and hence, multiphase accretion flow (Yuan 2003). The existence of such cold clouds embedded in hot accretion discs is now confirmed as the broad-line region (BLR), which successfully explains some of the observational evidence. Gillessen et al. 2012; Burkert et al. 2012 have shown that even near the Galactic Centre, there are some clouds in orbit around the central supermassive black hole. On the other hand, some numerical simulation clearly shows the formation of cold, dense clumps, likely due to thin-shell instabilities in the shocks formed by the stellar winds (e.g. Vishniac 1994). Our Galactic Centre, Sgr A∗, is surrounded by young, massive stars. Some of these stars are in the Wolf–Rayet phase and have mass-loss rates that could be as high as $10^{-4} \, M_\odot \, yr^{-1}$. One of these clumps could correspond to the G2 cloud, which was discovered

[*] E-mail: abbassi@um.ac.ir

on its way to being tidally sheared by Sgr A∗ (Gillessen et al. 2012, 2013). Furthermore, there is strong evidence from both theoretical and observational works that imply accretion on to some black hole X-ray binaries (BHXB; Malzac & Celotti 2002; Merloni et al. 2006), AGN (Kuncic, Blackman & Rees 1996; Kumar 1999), including low-luminosity AGNs (Celotti & Rees 1999), and ultra-luminous X-ray sources are clumpy rather than homogeneously continuous. Several instabilities driven by thermal (Krolik 1998), magnetorotational (Blaes & Socrates 2001, 2003), and photon bubble (Gammie 1998) have been reported in accreting systems. In the innermost region of BHXBs, the hard X-ray includes broad iron lines and thermal radiation, which are unusual for such a hot fully ionized gas. This strange spectrum can be explained by the existence of cold clumps (Yu et al. 2018). Recent infrared observations have identified low-mass gas clouds, G1 and G2, moving through this exact region. Measuring their interaction with the background gas could, therefore, provide important information about black hole accretion physics (e.g. Narayan, Ozel & Sironi 2012).

Current attempts to study these clumpy systems concentrate on answering these main aspects: Understanding the processes that may lead to the formation of BLR clouds is an active research field (e.g. Fromerth & Melia 2001; Pittard et al. 2003). Moreover, there are noticeable uncertainties about the stability of these clouds and the confinement mechanisms in the light of theoretical arguments and recent numerical simulations (Rees 1987; Krause, Schartmann & Burkert 2012; Namekata, Umemura & Hasegawa 2014). Regardless of any current uncertainty over the nature of the confinement mechanisms, the orbital motion of BLR clouds and their radiated emission allow us to estimate the mass of the central black hole (e.g. Marconi et al. 2008; Netzer & Marziani 2010).

So far, the spectral properties of clumpy accretion flows are investigated by some authors like Guilbert & Rees (1988), Malzac & Celotti (2002), Merloni et al. (2006), and Krolik (1998). The dynamics of cold clumps inside ADAFs between the tidal disruption radius and the transition radius are studied by Wang, Cheng & Li (2012) (WCL12). They could find analytical solutions for both strong and weak coupling between clumps and ADAF. Ghayuri (2016) studied the BLRs by using Jean's equations in cylindrical coordinates. He obtained the distributions of cold clumps that can be found in three configurations of non-disc, disc-wind, and pure disc. Khajenabi, Rahmani & Abbassi (2014), followed WCL12 and took into account the magnetic field effects on clumps' dynamics due to clumps' strong coupling to their ambient medium. In fact, the magnetic field is very important to keep clumps close to the central region of AGNs (Rees 1987).

One of the main ingredients of previous theoretical (or simulation) studies is the true nature of the intercloud medium. The complete physics of these clouds is highly complex and involves several physical processes such as pressure, radiative, centrifugal, gravitational, and magnetic forces; consequently, our knowledge about the intercloud medium is still poor. Most of the previous analytical studies of BLR clouds are based on a few certain simplifying approximations. Recently, it has been suggested by Krause, Schartmann & Burkert (2011) that one of the plausible candidates to describe the intercloud medium is ADAFs, where the pressure of the gas varies in proportion to a power-law function of the radial distance (e.g. Narayan & Yi 1994). Das & Sharma (2013) and Bu & Gan (2018) have found that cold clumps can coexist with hot accretion flow. Simulation performed by Bu & Gan (2018) has shown that the accretion rate increases to a value at which the radiative cooling rate is roughly equal to or slightly larger than the viscous heating rate, and cold clumps can form around the equatorial plane. On the other

hand, Burkert et al. (2012) performed numerical simulations of a clumpy cloud with properties similar to G2, which is moving within the ambient gaseous medium and is modelled as an ADAF. They found that despite the variations of the cloud due to its interactions with the ambient gaseous medium the cloud preserves its pressure equilibrium with the surrounding medium (also see, Scharmann et al. 2008). Cloud stability and confinement require them to be in rough pressure equilibrium with their environment (e.g. Krolik, McKee & Tarter 1981; Krolik 1988). To reach the required pressure of $p \approx 10^{-2}$ dyne cm^{-2}, the intercloud medium needs either a high temperature ($\approx 10^7$ K; Krolik 1988), following the above-mentioned papers, here we also describe intercloud medium using an analytical model of ADAFs. In an extremely low-accretion rate, the collisional mean free path of electrons is large compared with the length-scale of the system, thus thermal conduction can have a significant influence on the dynamics of the accretion flow. On the other hand, in ADAFs, the temperature of the flow is near-virial, and the internal energy of particles is very large. Therefore, the extra heat which could not be transported outwards via radiation cooling should be carried through other ways like advection. Besides advection, conduction can transport heating in the radial direction. Tanaka & Menou (2006) investigated the effect of thermal conduction in ADAFs for the first time. Their work was followed by Shadmehri (2008), Abbassi, Ghanbari & Najjar (2008), and Abbassi, Ghanbari & Ghasemnezhad (2010) to find how the dynamics of flow change in the presence of conduction.

In the paper on WCL12, the clumps are treated as stable long-lived objects and because of that the time dependency of quantities is ignored. However, besides the stationary configuration of clumps, another approach can be followed based on the transient nature of cold clouds. In fact, time evaluation of clumps is an effective tool for finding the population properties of BLRs of AGN. BLRs are believed to consist of dense clumps of hot gas in a much hotter diluted medium such as ADAFs and the motion of clouds has the main role in broadening their emission lines. Moreover, the existence of clumps in BLR has been proved by spect-polarimetric observations, too (Smith et al. 2005; Ghayuri 2016).

In order to obtain precious information about the structure of AGN and provide an estimation for the mass of the central black hole (e.g. Marconi et al. 2008; Netzer & Marziani 2010), orbital analysis of BLR clouds has attracted some author's attention (Krause et al. 2011; Plewa, Schartmann & Burkert 2013; Shadmehri 2015; Khajenabi 2015, 2016). To study BLR clouds, it is common to assume the clumps have balanced interior pressure with their ambient pressure. Therefore, a cloud with a fixed mass that is subject to the gravity of the central black hole and the friction force can be treated in the format of a classical two-body problem. Some works, such as Mittleman & Jezewski (1982), Mavraganis & Michalakis (1994), Humi & Carter (2002), Shadmehri (2015), and Khajehnabi (2016) have been done by following this approach. In these papers, a power-law pressure distribution for the inter-clouds medium has been applied. The common result of all these works is that irrespective of initial conditions or the form of friction force orbital decay occurs in such systems because of considering the drag force. Shadmehri (2015) has introduced the time-of-flight as the estimated time for a cloud needs to fall on to the central region. He found that the drag force coefficients are important in the flight time of a BLR cloud and change it linearly.

Now in this paper, we first work on the ensemble of clumps and employ the collision-less Boltzman equations to describe their dynamics. In Section 2, we write the basic equations in cylindrical coordinates and simplify them by assuming ignorable vertical move-

ment for both clumps and the ambient medium. As we know (from WCL12) in the case of strong coupling, the averaged properties of clumps follow the ADAF dynamics. Therefore, both the average velocity of clumps and drag force will be affected by thermal conductivity in the intercloud gas. That is why we pay special attention to the characteristics of an ADAF possessing thermal conductivity in Section 3. The result of sections 2 and 3 are combined in Section 4 for finding the velocity dispersion between the clumps and the ADAF. For the second part of this work and in Section 5, we study the dynamics of clumps individually just like the two-body problem, and write the momentum equation for two directions (radial and azimuthal) at the equatorial plane. We will use the same formula for drag force as the first part, and see how much the trajectory of a BLR cloud changes by adding thermal conduction. And finally, the summary and conclusion are presented in Section 6.

2 BASIC EQUATIONS AND ASSUMPTIONS

As we stated in the introduction existence of cold clouds embedded in hot accretion discs is now confirmed as the BLR, which successfully explains the observational evidence. The formation of cold clouds can be simply justified by thermal instability (TI). Although the detailed calculation of thermal instability is beyond the scope of this paper, we may use simplified arguments to grasp some essential properties of cold clouds. The Maximum size of the cold clump is specified by crossing the distance of a sound wave within one Keplerian time-scale. Typical values for mass and radius of clump, $m_{cl} = 4 \times 10^{24}$ g and $R_{cl} = 10^{11}$ cm, in the case, we have a supermassive central black hole with 10^8 M$_\odot$ (table 1, WCL12). We may expect that the size and mass of the clumps change with the radial distances to the black hole. On the other hand, the energy transport (cooling and heating of the clump) will specify the minimum size of the clump, below which the clump will be evaporated (WCL12). Furthermore, Sutherland & Dopita (1993) have shown that due to efficient line cooling clump temperature could retain a constant value around $T = 10^4$ K.

One more concern is whether this clump can remain unchanged and survive in an ADAF. Actually, turbulence in the accretion disc can not destroy these clumps. MRI or any other mechanism for turbulence in the discs is only a small disturbance to the clump, since the clump size is much smaller than the typical length of turbulence. Moreover, the small turbulence eddies whose size is comparable to the clump have very small kinetic energy according to Kolmogorov's law (Landau & Lifshitz 1959). Considering all of these arguments, it would be an acceptable approximation that clumps are simplified as particles. Furthermore, if we assume a specific volume for any individual clump, we need to take the tidal force into the account especially close to the black hole, which may disrupt the clumps. As an approximation for simplifying the complexity of the problem in this study, we assume BLR clouds as a system of point-like particles. So, we may ignore the effect of tidal interactions. WCL12 has shown that in clumpy-ADAF system collision, the clumps can be neglected. So it is worth assuming the clumps as a system of collision-less particles were moving inside the ADAFs. Therefore, we need to apply the Boltzmann equation.

Boltzmann equation works with the state of the gas statistically. First, we define the distribution function, $f(\mathbf{x}, \mathbf{v}, t)$ such that $f\,\mathrm{d}^3x\,\mathrm{d}^3v$, which is the average number of particles contained in a volume element d^3x about x, and a velocity-space element d^3v about v at time t. Macroscopic properties of the gas such as the number density of the particles, n, and the average velocity of an element of gas u (= macroscopic flow velocity) can be evaluated from this function as:

$$n(\mathbf{x}, t) = \int_{-\infty}^{+\infty} f(\mathbf{x}, \mathbf{v}, t)\,\mathrm{d}^3v, \tag{1}$$

$$u(\mathbf{x}, t) = n^{-1} \int_{-\infty}^{+\infty} f(\mathbf{x}, \mathbf{v}, t)\mathbf{v}\,\mathrm{d}^3v = \langle v \rangle, \tag{2}$$

The distribution function in the absence of collisions is invariant, so we recast the Boltzmann equation as:

$$F = \frac{\partial f}{\partial t} + v^i \frac{\partial f}{\partial x^i} + a^i \frac{\partial f}{\partial v^i} = 0, \tag{3}$$

where a^i is the i-component of the acceleration vector (due to the external force $F(\mathbf{x}, t)$, such that $a(\mathbf{x}, t) = F(\mathbf{x}, t)/m$, where m is the mass of a single particle). Equation (3) is known as the collision-less Boltzmann equation, or Vlasov's equation. The equations of fluid dynamics can be derived by calculating moments of the Boltzmann equation for quantities that are conserved in collisions of the particles. Regarding clumps which are assumed to be collision-less, we require the moments of the Boltzmann equation obtained from equation (3) and simplifying $\int n F\,\mathrm{d}^3v = 0$ that yield:

the zero moments:

$$\frac{\partial n}{\partial t} + \frac{\partial}{\partial x_i}(n\langle v_i \rangle) = 0, \tag{4}$$

and the first moment:

$$\frac{\partial}{\partial t}(n\langle v_i \rangle) + \frac{\partial}{\partial x_i}(n\langle v_i v_j \rangle) - n\langle a_j \rangle = 0. \tag{5}$$

Now converting the Cartesian coordinates to cylindrical coordinates, equations (4) becomes:

$$\frac{\partial n}{\partial t} + \frac{1}{R}\frac{\partial}{\partial R}(Rn\langle v_R \rangle) + \frac{1}{R}\frac{\partial}{\partial \phi}(n\langle v_\phi \rangle) + \frac{\partial}{\partial z}(n\langle v_z \rangle) = 0, \tag{6}$$

and the three components of vectorial equation (5) are found as:

$$\frac{\partial}{\partial t}(n\langle v_R \rangle) + \frac{1}{R}\frac{\partial}{\partial R}\left(Rn\langle v_R^2 \rangle\right) + \frac{1}{R}\frac{\partial}{\partial \phi}\left(n\langle v_R v_\phi \rangle\right)$$
$$+ \frac{\partial}{\partial z}(n\langle v_R v_z \rangle) - n\langle a_R \rangle - n\frac{\langle v_\phi^2 \rangle}{R} = 0, \tag{7}$$

$$\frac{\partial}{\partial t}\left(n\langle v_\phi \rangle\right) + \frac{1}{R^2}\frac{\partial}{\partial R}\left(R^2 n\langle v_R v_\phi \rangle\right)$$
$$+ \frac{1}{R}\frac{\partial}{\partial \phi}\left(n\langle v_\phi^2 \rangle\right) + \frac{\partial}{\partial z}(n\langle v_\phi v_z \rangle) - n\langle a_\phi \rangle = 0, \tag{8}$$

$$\frac{\partial}{\partial t}(n\langle v_z \rangle) + \frac{1}{R}\frac{\partial}{\partial R}(Rn\langle v_R v_z \rangle)$$
$$+ \frac{1}{R}\frac{\partial}{\partial \phi}(n\langle v_R v_z \rangle) + \frac{\partial}{\partial z}\left(n\langle v_z^2 \rangle\right) - n\langle a_z \rangle = 0, \tag{9}$$

after applying assumptions of $\partial/\partial t = \partial/\partial \phi = 0$ and also neglecting the terms including: $\langle v_z \rangle$, $\langle v_R v_z \rangle$, and $\langle v_\phi v_z \rangle$, we have:

$$\frac{1}{R}\frac{\partial}{\partial R}(Rn\langle v_R \rangle) = 0, \tag{10}$$

$$\frac{1}{R}\frac{\partial}{\partial R}\left(Rn\langle v_R^2 \rangle\right) - n\langle a_R \rangle - n\frac{\langle v_\phi^2 \rangle}{R} = 0, \tag{11}$$

$$\frac{1}{R^2}\frac{\partial}{\partial R}\left(R^2 n\langle v_R v_\phi \rangle\right) - n\langle a_\phi \rangle = 0, \tag{12}$$

$$\frac{\partial}{\partial z}\left(n\langle v_z^2 \rangle\right) - n\langle a_z \rangle = 0, \tag{13}$$

In equations (11)–(13), we see the acceleration's components, a_i, which are specified by two factors: first, gravitational potential $\psi = -GM/(R^2 + z^2)^{1/2}$ and secondly drag force, $D_i = -f_i(v_i - V_i)|v_i - V_i|$, where V_i and $f_i (> 0)$ are ADAF velocity component
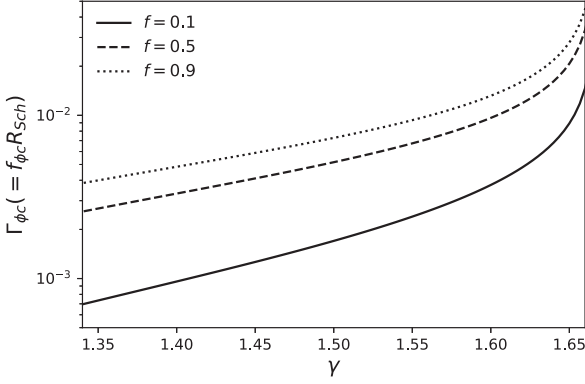
Figure 1. Critical value of rotational drag force coefficient with respect to the polytropic parameter with different f's.

and coefficient of drag force per unit mass, respectively. Here, it is necessary to determine the sign of drag force:

$$D_i = \begin{cases} +f_i(v_i - V_i)^2 > 0 & \text{if} \quad v_i < V_i \\ -f_i(v_i - V_i)^2 < 0 & \text{if} \quad v_i > V_i \end{cases}. \tag{14}$$

As we mentioned before in the current work, we assume that clumps have been strongly coupled with their hot medium. Accordingly, the averaged value of D_i is estimated by applying this approximation: $\langle v_i \rangle = V_i$, and thus the averaged acceleration of drag force can be simplified as:

$$\langle D_i \rangle = -f_i \left(\langle v_i^2 \rangle - V_i^2 \right). \tag{15}$$

Notice that we use the above formula for both cases of $v_i < V_i$ and $v_i > V_i$. To explain equation (15), first, according to equation (14), D_i can be negative (if $v_i > V_i$) or positive (if $v_i < V_i$), hence it sounds logical not to expect the sign of $\langle D_i \rangle$ becomes different from D_i itself (since in strong coupling, most of clumps must rotate in the same direction of ADAF and moves inwards to join the accretion process), and secondly it seems reasonable to consider $v_i^2 < V_i^2$ for the first case and $v_i^2 > V_i^2$ for the second case (again because of their similar direction of movements for strong coupling). Consequently, to estimate the approximate value of $\langle D_i \rangle$, we need to note that:

$$\langle (v_i - V_i)^2 \rangle \approx \begin{cases} V_i^2 - \langle v_i^2 \rangle & \text{if} \quad v_i < V_i \\ \langle v_i^2 \rangle - V_i^2 & \text{if} \quad v_i > V_i \end{cases}.$$

Now we are able to achieve the average value of total acceleration components:

$$\langle a_R \rangle = -\frac{v_K^2}{R} - f_R \left(\langle v_R^2 \rangle - V_R^2 \right), \tag{16}$$

$$\langle a_\phi \rangle = -f_\phi \left(\langle v_\phi^2 \rangle - V_\phi^2 \right), \tag{17}$$

$$\langle a_z \rangle = -\frac{z}{R^2} v_K^2 - f_z \langle v_z^2 \rangle, \tag{18}$$

where $v_K^2 = GM/(R^2 + z^2)^{1/2} \approx GM/R^3$, and we have assumed that $V_z = 0$, $V_R = \langle v_R \rangle$, and $V_\phi = \langle v_\phi \rangle$.

Let us back to equation (10), using the approximation of $\langle v_R \rangle = V_R$, we can find the radius dependency of clumps' density as:

$$n = n_0 \left(\frac{R}{R_0} \right)^{-3/2}, \tag{19}$$

where n_0 is the density of clumps estimated in the typical radius of R_0. Notice that NY94 solved the height-averaged equations of ADAFs, the same result is seen here by integrating the differential equation (19) along vertical direction of z and assuming $H \propto R$, or
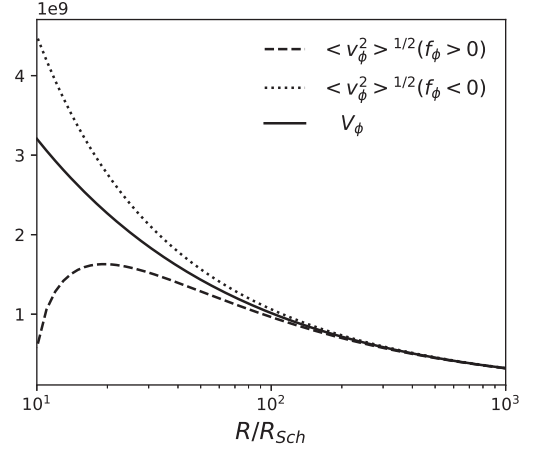

Figure 2. Variation of the rotational velocity squared as a function of radius, r. In this figure, the parameters are: $f = 0.9$, $\alpha = 0.1$, $\gamma = 1.4$, and $f_\phi R_{\text{Sch}} = \Gamma_\phi = \pm 5 \times 10^{-3}$, where $R_{\text{Sch}} = 2.95 \times 10^5 m_*$ (cm) is the Schwarzschild radius.
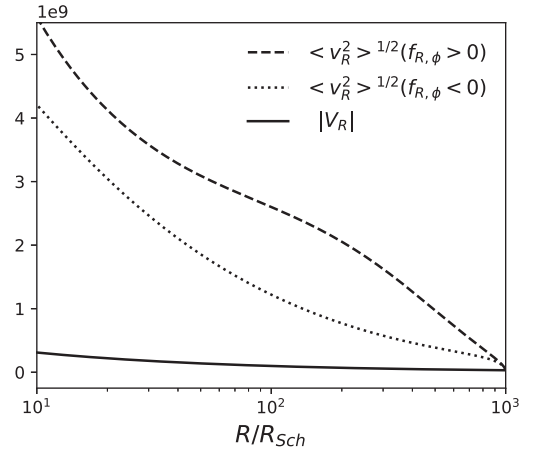

Figure 3. Variation of the radial velocity squared as a function of radius, R. In this figure, the parameters are: $f = 0.9$, $\alpha = 0.1$, $\gamma = 1.4$, $f_{R, \phi} R_{\text{Sch}} = \Gamma_{R, \phi} = \pm 5 \times 10^{-3}$.

else, we would find $n \propto R^{-1/2}$ like Ghayuri (2016, see equation 22 of his paper). The height integrated version of continuity equation yields the constant mass accretion rate for clumps as:

$$\dot{M}_{\text{cl}} = -2\pi R H n m_{\text{cl}} \langle v_R \rangle, \tag{20}$$

where m_{cl} is the average mass of individual clumps, and H is the half-thickness of medium in R radius, which can be approximated by R for an ADAF, i.e. $H \sim R$. Substituting $\langle a_\phi \rangle$ and n from equations (17) and (19) in the second equation of momentum and approximating $\langle v_R v_\phi \rangle \approx V_R V_\phi$, equation (12) gives:

$$\langle v_\phi^2 \rangle = V_\phi \left(V_\phi + \frac{V_R}{2Rf_\phi} \right). \tag{21}$$

Since $V_R < 0$, we might expect $\langle v_\phi^2 \rangle < V_\phi^2$ (see Fig. 2, compare two curves marked by dashed and solid lines). In addition, we should notice that $\langle v_\phi^2 \rangle$ becomes smaller towards the centre, and somewhere it might become zero with a critical value of f_ϕ:

$$\Gamma_{\phi c} = -\frac{V_R}{2r_{\text{in}} V_\phi} = \frac{3\alpha}{2\sqrt{2\epsilon'(5 + 2\epsilon')}r_{\text{in}}}, \tag{22}$$

where $\Gamma_{\phi c} = f_{\phi c} R_{\rm Sch}$, ($R_{\rm Sch}$ is the Schwarzschild radius), and like NY94 for convenience, we have defined the parameter of ϵ' instead of $(5/3 - \gamma)/[f(\gamma - 1)]$, and also scaled inner radius as: $r_{\rm in} = R_{\rm in}/R_{\rm Sch}$.

This critical value of Γ_ϕ is similar to equation (26) of WCL12, but independent of the radius and only changes by previously known parameters of this problem, i.e. α, γ, f, and $r_{\rm in}$. In Fig. 1, we have shown $\Gamma_{\phi c}$ as a function of γ for different f's and a constant α (= 0.1).

The last achievable quantity here is $\langle v_R^2 \rangle$ appeared in equation (11). In Fig. 3 the variation of the radial velocity squared as a function of radius, R have been illustrated. This equation can be simplified by substituting $\langle a_R \rangle$ and $\langle v_\phi^2 \rangle$ from equations (16) and (21). So we have:

$$\frac{d\langle v_R^2 \rangle}{dR} - \frac{1}{2R}\langle v_R^2 \rangle + \frac{v_K^2}{R} + f_R \left(\langle v_R^2 \rangle - V_R^2 \right) - \frac{V_\phi}{R}\left(V_\phi + \frac{V_R}{2Rf_\phi} \right) = 0.$$

It will be more convenient, if we use $R_{\rm Sch}$ as a length-scale and convert R to r (= $R/R_{\rm Sch}$). So by multiplying the above equation by $R_{\rm Sch}$, and applying the definition of $\Gamma_i = f_i R_{\rm Sch}$, we find:

$$\frac{d\langle v_R^2 \rangle}{dr} - \frac{\langle v_R^2 \rangle}{2r} + \frac{v_K^2}{r} + \Gamma_R \left(\langle v_R^2 \rangle - V_R^2 \right) - \frac{V_\phi}{r}\left(V_\phi + \frac{V_R}{2r\Gamma_\phi} \right) = 0. \quad (23)$$

If we write the velocity components of ADAF as: $V_i = c_i v_K(r)$, we can obtain the following result by solving the above equation:

$$\langle v_R^2 \rangle = c_K^2 r^{1/2} e^{-\Gamma_R r} \left\{ C_1 + c_R^2 \Gamma_R \int_r^{r_f} r^{-3/2} e^{\Gamma_R r} dr \right.$$
$$\left. - (1 - c_\phi^2) \int_r^{r_f} r^{-5/2} e^{\Gamma_R r} dr + \frac{c_R c_\phi}{2\Gamma_\phi} \int_r^{r_f} r^{-7/2} e^{\Gamma_R r} dr \right\}, \quad (24)$$

where $c_K^2 = GM/R_{\rm Sch} (= c^2/2)$ and C_1 is a constant value, which can be obtained from this boundary condition: $\langle v_R^2 \rangle |_{r_f} = V_R^2 |_{r_f}$ ($r_f = 1000 R_{\rm Sch}$ is the outer boundary where the ADAF solutions are satisfied) then we find,

$$C_1 = c_R^2 r_f^{-3/2} e^{\Gamma_R r_f},$$

with using c_R, c_ϕ, and c_K, equation (21) changes as below:

$$\langle v_\phi^2 \rangle = c_\phi \left(c_\phi + \frac{c_R}{2r\Gamma_\phi} \right) c_K^2 r^{-1}. \quad (25)$$

In the next section, we will find the constants of c_R and c_ϕ for an ADAF with thermal conduction.

3 ADAF SOLUTIONS WITH THERMAL CONDUCTION

We are interested in analysing the structure of ADAF, where thermal conduction plays an important role in energy transportation. Here, we write the basic conservation equations for an ADAF with the same assumptions as NY94, and involve the thermal conduction term in energy equation (Tanaka & Menou 2006). We assumed a steady axisymmetric accretion flow, $\frac{\partial}{\partial t} = \frac{\partial}{\partial \phi} = 0$. We can write the standard equations in the cylindrical coordinates (r, ϕ, z). In addition, we vertically integrate the flow of equations, and therefore, all the physical variables become only the functions of radial distance r. Moreover, relativistic effects are neglected and Newtonian gravity in the radial direction is taken into account. The simplified form of radial and azimuthal components of momentum equation and energy equation are presented in the three following equations:

$$V_R \frac{dV_R}{dR} = \frac{V_\phi^2 - v_k^2}{R} - \frac{1}{\rho}\frac{d(\rho C_s^2)}{dR}, \quad (26)$$

$$V_R \frac{d(RV_\phi)}{dR} = \frac{1}{\rho R H}\frac{d}{dR}\left[\frac{\alpha \rho C_s^2 R^4 H}{v_k}\frac{d}{dR}\left(\frac{V_\phi}{R} \right) \right], \quad (27)$$

$$2H\rho V_R T \frac{ds}{dR} = f\frac{2\alpha \rho C_s^2 R^3 H}{v_k}\left[\frac{d}{dR}\left(\frac{V_\phi}{R} \right) \right]^2 - \frac{2H}{R}\frac{d(RF_s)}{dR}, \quad (28)$$

where T, s, and f are the temperature, entropy, and advection parameter, respectively; and $H = RC_s/v_K$ is the vertical thickness of hot accretion flow, $F_s = 5\Phi_s \rho C_s^3$ is the saturated conduction flux (Cowie & McKee 1977), and Φ_s is the saturation constant, respectively. According to the self-similar method for the radial direction, all quantities with velocity dimension should be proportional to $R^{-1/2}$ and density is assumed to be proportional to $R^{-3/2}$. Consequently, equations (26)–(28) give us,

$$c_\phi^2 = 1 - \frac{1}{2}c_R^2 - \frac{5}{2}c_s^2, \quad (29)$$

$$c_R = -\frac{3}{2}\alpha c_s^2, \quad (30)$$

$$\frac{9}{8}\alpha^2 c_s^4 + \left[\frac{5}{2} + \frac{5 - 3\gamma}{3f(\gamma - 1)} \right] c_s^2 - \frac{40\Phi_s}{9\alpha f}c_s - 1 = 0 \quad (31)$$

where $c_{R,\phi} = V_{R,\phi}/v_K$ and $c_s = C_s/v_K$. As seen, there are three unknown variables, i.e. c_R, c_ϕ, and c_s^2 in the above equations, which can be found numerically. Now, we first solve the algebraic equation (31) in order to find c_s^2, and secondly we substitute the solution of c_s^2 in equation (29), which has been simplified as below by applying equations (30) and (31):

$$c_\phi^2 = \frac{5 - 3\gamma}{3f(\gamma - 1)}c_s^2 - \frac{40\Phi_s}{9\alpha f}c_s.$$

Notice that substituting some values of Φ_s in the solutions yields $c_\phi^2 < 0$ (this issue has been discussed in Ghasemnezhad, Khajavi & Abbassi 2012). This point will be clarified better by looking at the contour plots in Fig. 4. This figure shows the variation of c_ϕ^2 with respect to Φ_s, and one of three other input parameters: α, f, γ in each subplot. In the first row panels of Fig. 4, the unacceptable region for c_ϕ^2 is located between two radial lines in the $\alpha - \phi_s$ plane, and it gets larger as the advection (in panel b) or polytropic parameter (in panel c) increases. The second three panels displays contour plots of c_ϕ^2 in $\gamma - \phi_s$ plane. The boundaries between negative and positive values of rotational velocity squared in the middle row panels are arc-shaped and placed on the right-upper side of panels (d)–(f). Comparing panel (d) with panel (e), a rise in advection causes an upward shift in the forbidden region. On the other hand, when comparing (d) with panel (f), we found out that when viscosity becomes stronger, the curved line of zero rotation seems flattered and moves to higher values of the thermal conduction parameter. Finally, the bottom panels of Fig. 4 present the behaviour of c_ϕ^2 by colours with changing ϕ_s and f. As seen, in each panel there is a vertical line with zero labels, which declares that choices of two input parameters of ϕ_s and f from the right of this line cannot result in a reasonable solution. Furthermore, the rectangular unacceptable part shrinks by greater viscosity (seen in panel i) but extends by growing γ. Consequently, in the light of this figure, we can find a proper value of ϕ_s for each certain set of input parameters (α, f, γ) to avoid forbidden areas.

In the following section, we will use these obtained solutions of the components of ADAF's velocity for finding drag force and calculating the root of the averaged radial and rotational velocities square.

4 THE EFFECT OF THERMAL CONDUCTION ON CLUMPY DISKS

In two previous sections, we reviewed momentum equations of clumpy ADAFs with different signs of drag force, and solved the simplified first-order differential equation of $\langle v_R^2 \rangle$ with respect to radial coordinate. The final result in equation (24) as a function of c_R and c_ϕ, i.e. coefficients of ADAF's velocity components in radial
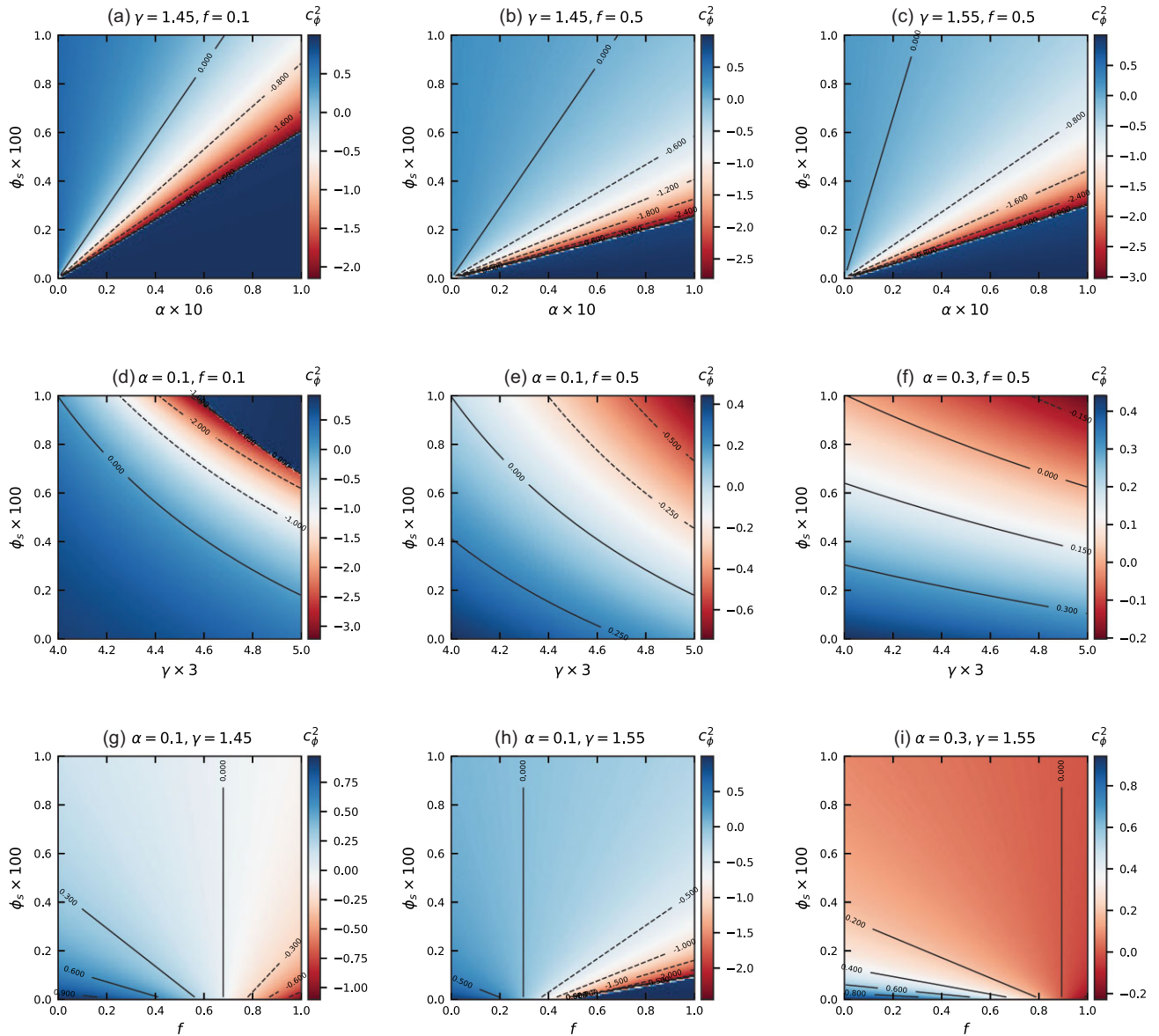
Figure 4. Variation of c_ϕ^2 showed by colours with the parameter of thermal conduction Φ_s, and one of three input parameters: α (a–c), f (d–f), γ (g–i). In this figure, the negative values of c_ϕ^2 are not physical, and we should carefully pick up a proper value of ϕ_s for each certain set of input parameters (α, f, γ) to avoid forbidden areas.

and azimuthal directions. Now, it is time to substitute the numerical ADAF solutions from equations (29)–(31) in equations (24) and (25). The results are illustrated in Figs 5 and 6. In these two figures, we have investigated the influence of thermal conduction on the dynamics of clumps for a different set of input parameters: (α, f, γ) in Fig. 5 and (Γ_R, Γ_ϕ) in Fig. 6. In these panels, we have considered $\Phi_s = 0.0005$, 0.002, and 0.004, remarked by dotted, dashed, and solid lines, respectively. In order to have an easier comparison, both velocity components of ADAF and clumps are presented in Figs 5 and 6. The velocity dispersion of clumps is presented in the main larger plots, and the small plots inside the main plots demonstrate the velocity of ADAF. Comparing the small and large plots declares that thermal conduction plays a similar role in changing the behaviour of clumps and ADAF.

The upper row panels of Figs 5, 6 show the behaviour of ADAFs (or equivalently approximated clumps' azimuthal velocity in small subplots inside the main plots) as well as the average rotational velocity square of clumps (in the bigger main plots). In all upper plots, grey curves show Keplerian velocity and assure us that the velocity dispersion in the azimuthal direction remains sub-Keplerian even after adding Φ_s. In this figure and Fig. 6, besides Φ_s, we have also examined two different values of each parameter, and we would like to investigate, in which circumstances, the effect of thermal conduction on the dynamics of the system becomes more significant. In Figs 5 and 6, we can easily see that the maximum variation of both components of velocity dispersion under the effect of thermal conduction occurs at the inner boundary of the ADAF (or equivalently at the captured radius of clumps) with each of these input parameters: α, γ, and f. Regardless of the value of each parameter, all these plots reveal that an increase of Φ_s reveals that the rotation of the hot medium will decrease as long as at the same time. It is also clear that this change in thermal conduction results in decreasing of the
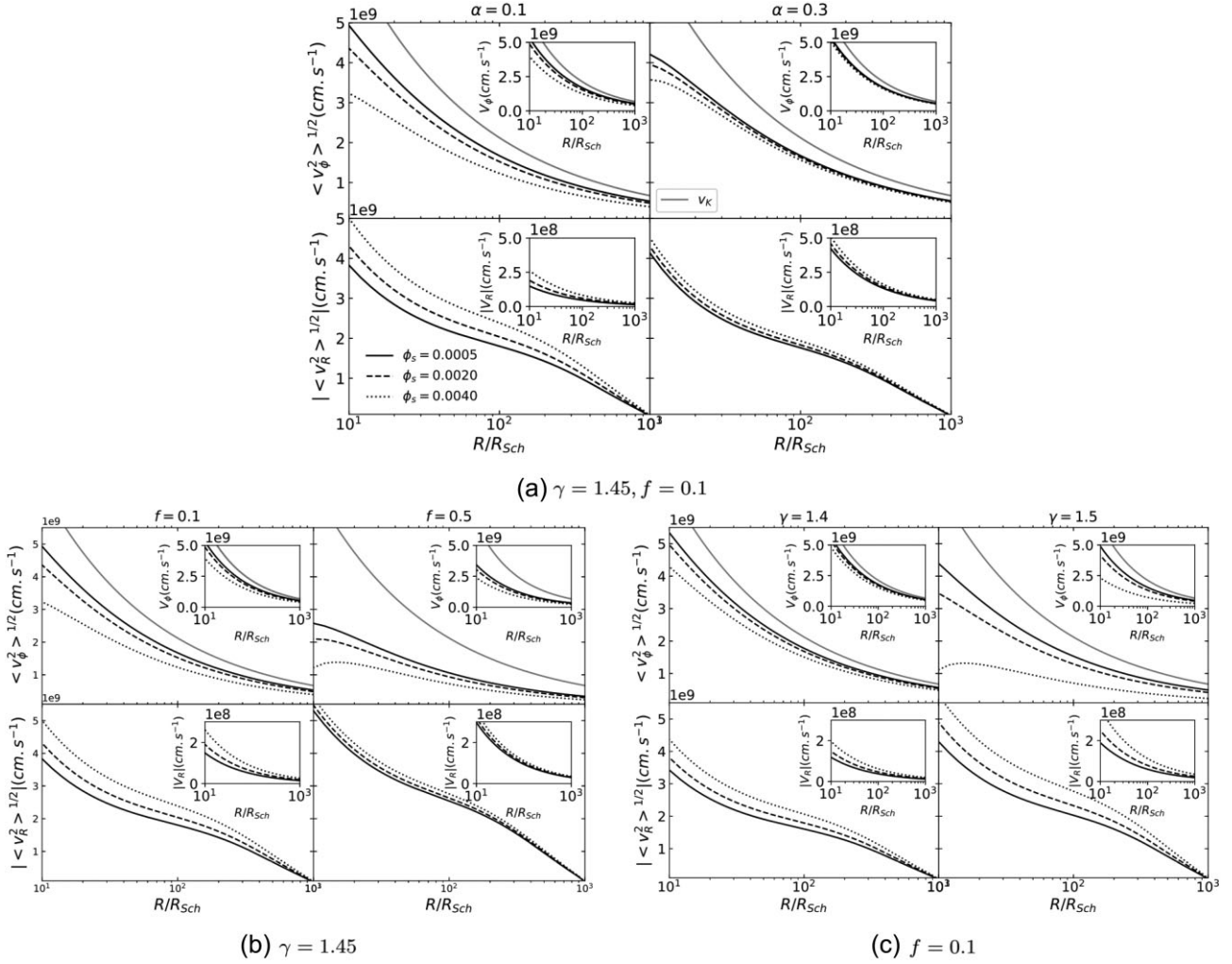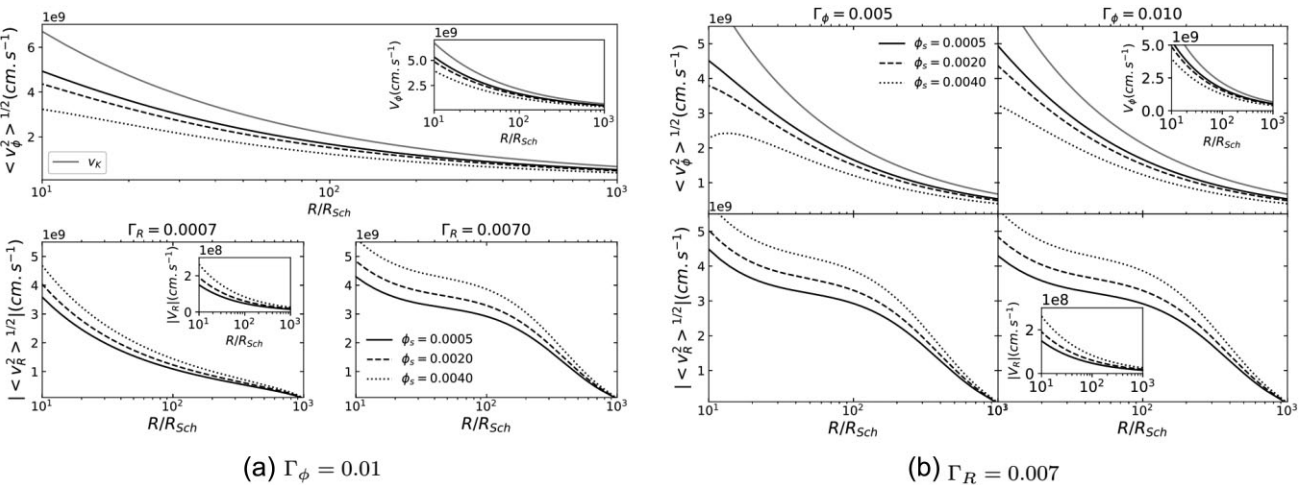
Figure 5. Solution of the clumpy-ADAF disc in the presence of thermal conduction: $\Phi_s = 0.0005$ (solid line), $\Phi_s = 0.0020$ (dashed line), $\Phi_s = 0.0040$ (dotted line). The three panels show the dependence of the solution on the three parameters α (panel a), f (panel b), and γ (panel c). All of these panels was set up for $\Gamma_R = 0.005$, $\Gamma_\phi = 0.01$.

Figure 6. Solution of the clumpy-ADAF disc in the presence of thermal conduction: $\Phi_s = 0.0005$ (solid line), $\Phi_s = 0.0020$ (dashed line), $\Phi_s = 0.0040$ (dotted line). The three panels show the dependence of the solution on the three-parameter Γ_R (panel a), in this panel we take $\Gamma_\phi = 0.01$, Γ_ϕ (panel b) when $\Gamma_R = 0.007$ and γ (panel c). All of this panels was set up for $\gamma = 1.45$, $f = 0.1$.

average rotational velocity square of clumps. Comparing upper right-hand panels with left ones leads us to know that $\langle v_\phi^2 \rangle^{1/2}$ remarkably decreases with increasing advection parameter and polytropic index, but does not behave uniformly with changing the viscosity parameter. Furthermore, according to Fig. 6 (two upper right-hand panels), an enhancement of the coefficient of drag force in ϕ-direction causes a bit increase in this quantity whereas changing of drag force in the radial direction (as we had seen in equation 25) does not have any direct effect on the average azimuthal velocity square of clumps. One more point to consider, if we look at the numbers of vertical axes of the main plots with ones in small plots, we realize that the velocity dispersion of clumps in the azimuthal direction and rotational velocity of ADAF possess the same order of magnitude.

The lower panels of Figs 5 and 6 display directly the role of thermal conduction in a variation of $\langle v_R^2 \rangle^{1/2}$ (presented in main bigger plots), and also in changing of V_R or $\langle v_R \rangle$ (presented in small subplots). According to these plots, we can find out unlike the Φ_s effect on velocity in the azimuthal direction, the total effect of Φ_s in the radial direction is positive on $\langle v_R^2 \rangle^{1/2}$ and also on $\langle v_R \rangle$. Here again, we catch our attention to the scale of vertical axes numbers: 10^9 for main plots and 10^8 for small subplots, so the radial velocity dispersion of clumps is about 10 times greater than V_R of ADAFs, this result is consistent with WLC12. Moreover, if we compare right-hand and left-hand panels in the bottom rows of each four-subplot shape, we notice that the difference between plots with the various value of Φ_s is more visible with smaller α and f but bigger γ and Γ_R. Finally, according to the four subplot shapes in the right-hand of Fig. 6, $\langle v_R^2 \rangle^{1/2}$ is not very sensitive to changing Γ_ϕ, which was pointed out in WLC12 too.

5 THERMAL CONDUCTION EFFECT ON THE PROJECTION OF CLUMPS

Up to now, we have been studying semi-analytically, the dynamical motion of clouds through the hot medium of ADAFs by adopting collision-less Boltzmann equation for the ensemble of clouds. Considering a more realistic picture, we may study the time-dependent orbits of such clouds as individual particles. In fact, the evaluation of the time-dependent trajectory of clumps informs us about the population properties of BLRs distributed around AGN. Therefore, for the rest of this paper, we work on the time-dependent dynamics of a simplified single-cloud model of clumps in the central vicinity of AGN. We aim to involve the thermal conduction term in the momentum equation. But for simplicity, we neglect the non-isotropic force due to the radiation of a central accretion disc. In this problem, we consider just two forces: the gravitational force of a central black hole with mass M, and a drag force involve between the clump and ADAF. This drag force is in the opposite direction of the cloud and its amplitude is proportional to square its relative velocity with respect to the ambient medium, i.e. ADAF. Thus, we can write the equations of the orbital motion as follows:

$$\ddot{R} - R\dot{\phi}^2 = -\frac{GM}{R^2} - f_R(\dot{R} - V_R)|\dot{R} - V_R|, \quad (32)$$

$$R\ddot{\phi} - 2\dot{R}\dot{\phi} = -f_\phi(R\dot{\phi} - V_\phi)|R\dot{\phi} - V_\phi|, \quad (33)$$

where $\dot{R} = \mathrm{d}R/\mathrm{d}t(= v_R)$, $\ddot{R} = \mathrm{d}^2R/\mathrm{d}t^2(= \mathrm{d}v_R/\mathrm{d}t)$, $\dot{\phi} = \mathrm{d}\phi/\mathrm{d}t(= v_\phi/R)$, and $\ddot{\phi} = \mathrm{d}^2\phi/\mathrm{d}t^2$. Like before, we have specified the velocity components of ADAF by V_R and V_ϕ, and we have also employed constant coefficients, f_R and f_ϕ for the components of drag force. For numerical evaluations, it seems more convenient to work with non-

dimensional quantities, hence we convert equations (32) and (33) to the non-dimensional forms by introducing r and τ as:

$$r = \frac{R}{R_0},$$
$$\tau = \frac{t}{t_0},$$

where R_0 and t_0 are the typical lengths and time-scales. We can take R_0 equal to the radial size of the background medium of BLR, that is the outer boundary of ADAF: $R_0 = 1000R_{\mathrm{Sch}}$[1]

Thus, the equations (32) and (33) become:

$$r'' - r\phi'^2 = -\frac{1}{r^2} - \Gamma_R \frac{R_0}{R_{\mathrm{Sch}}} \left(r' - \frac{c_R}{\sqrt{r}} \right) \left| r' - \frac{c_R}{\sqrt{r}} \right|, \quad (34)$$

$$r\phi'' - 2r'\phi' = -\Gamma_\phi \frac{R_0}{R_{\mathrm{Sch}}} \left(r\phi' - \frac{c_\phi}{\sqrt{r}} \right) \left| r\phi' - \frac{c_\phi}{\sqrt{r}} \right|, \quad (35)$$

where $r' = \mathrm{d}r/\mathrm{d}\tau$, $r'' = \mathrm{d}^2r/\mathrm{d}\tau^2$, $\phi' = \mathrm{d}\phi/\mathrm{d}\tau$, and $\phi'' = \mathrm{d}^2\phi/\mathrm{d}\tau^2$, the two constants of c_R and c_ϕ refer to the radial and azimuthal components of the velocity vector of ADAF. Also in the two above equations, we have removed the factor of GM in the gravitational term by choosing $t_0 = \sqrt{R_0^3/GM}$. Moreover, we have substituted $\Gamma_R/R_{\mathrm{Sch}}$ and $\Gamma_\phi/R_{\mathrm{Sch}}$ instead of f_R and f_ϕ. Now, we need to specify appropriate initial conditions for solving numerically the last two equations. In the absence of radiation force from the central object and neglecting the vertical component of the velocity vector of the ambient medium, i.e. ADAF, $v_z = 0$, we may expect the plane of motion to be fixed at the equatorial plane. However, under the influence of drag force, the cloud's angular momentum cannot remain constant (during flight time). So we expect a spiral trajectory for the cloud's motion.

Regarding boundary conditions, we assume that our single cloud begins its journey from the initial point with these dimensionless coordinates: ($r = 1$, $\phi = 0$) with an initial velocity vector equals to ADAF's one, i.e. ($r' = c_R$, $\phi' = c_\phi$). Knowing the initial conditions for r, ϕ, r', and ϕ', we can solve equations (34) and (35) numerically with respect to the dimensionless time, τ, and obtain $r(\tau)$, $\phi(\tau)$, $r'(\tau)$, and $\phi'(\tau)$. In Fig. 7, we have drawn the orbit of a sample cloud at the equatorial plane for three values of ϕ_s. The black dot–dashed, blue dashed, and red solid lines correspond to $\phi_s = 0$, 0.002, and 0.004, respectively, and the other input parameters for panels (a)–(c) are $\alpha = 0.2$, $f = 0.1$, and $\gamma = 1.4$; for panels (d)–(f): $\alpha = 0.1$, $\Gamma_\phi = \Gamma_R = 0.001$. Regarding the two remained parameters, one of them is variable and the other one is common for two adjacent panels. The label of τ_f in each panel (exception for panel f) is a dimensionless time that the BLR cloud needs for one rotation around the centre in the case of $\phi_s = 0$. For panel (f), this duration is too long for the cloud in a medium with $\phi_s = 0.004$, since during a smaller time, it arrives at the capture radius, hence in the case (i.e. $\phi_s = 0.004$), we have used the total flight time of the cloud, i.e. $\tau_T (= 1.56)$ instead of $\tau_f (= 2.03)$.

As it is seen in all panels of this figure, the motion of the cloud is a spiral around the centre, and this common feature appears due to the influence of drag force in this problem. Moreover, we see in all panels that thermal conduction apparently causes the clump to rotate and accrete faster. In Fig. 8, we have adopted the same input parameters, and for a better and easier comparison, we have chosen the same time flight for all cases (except for a grey line of panel c), and separated curves with equal values for ϕ_s. The effect of parameters other than ϕ_s can be studied more conveniently in this figure. By

---

[1]Notice that the dimensionless radius of r is three orders of magnitude larger than the previous quantity of r used in equations (23)–(25).
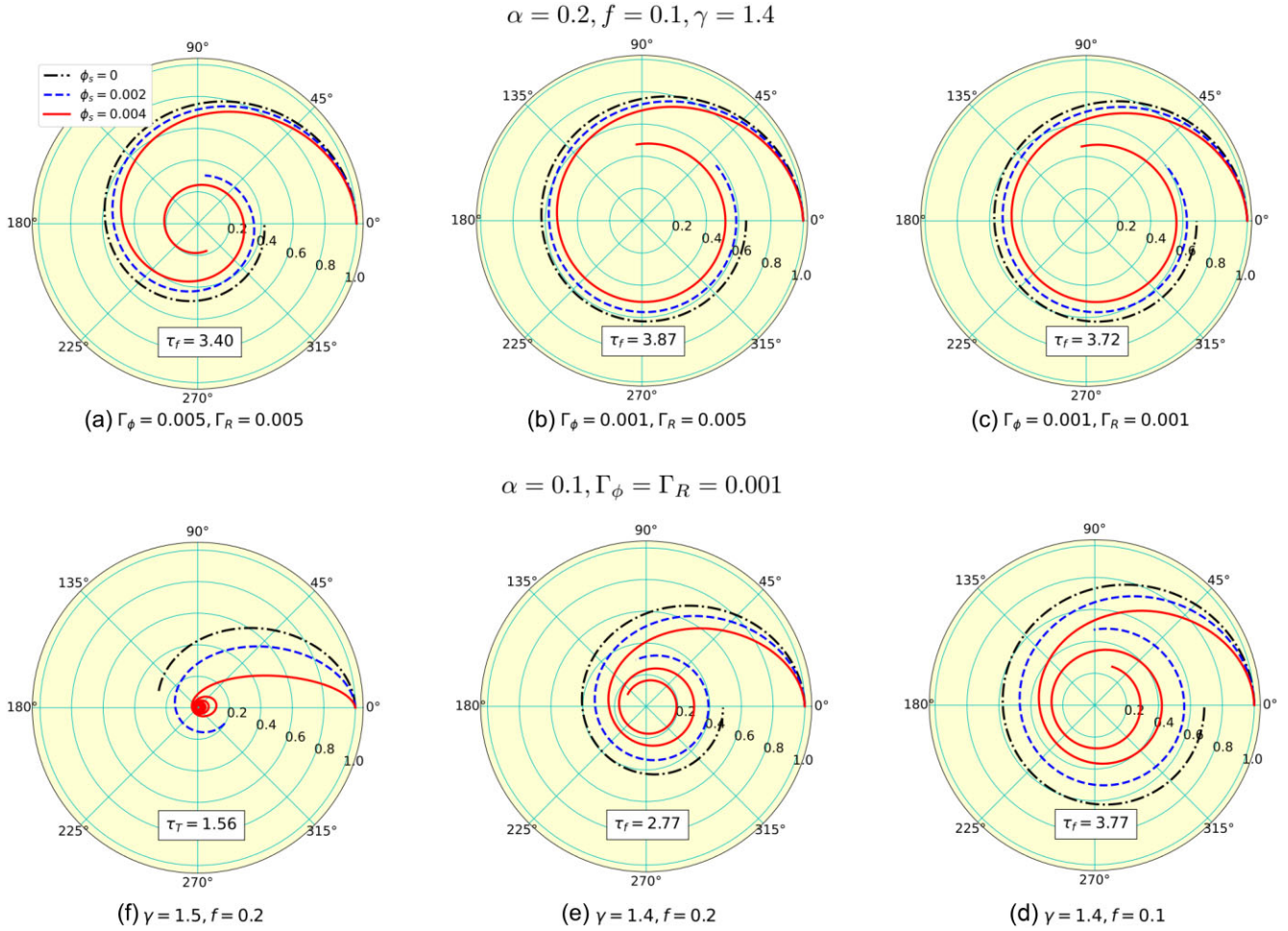
Figure 7. The effect of thermal conduction on the orbital motion of a clump embedded in an ADAF. In this figure, we have neglected the radiation force from the central object, thus the BLR cloud here moves only at the equatorial plane. In each panel, we have fixed the set of input parameters and examined three different values of the thermal conduction parameter, i.e. $\phi_s = 0, 0.002, 0.004$. In the upper panels, we have used: $\alpha = 0.2, f = 0.1, \gamma = 1.4$, and in the bottom panels: $\alpha = 0.1, \Gamma_R = \Gamma_\phi = 0.001$. Initial conditions are: $r|_{t=0} = 1$ (or $R|_{t=0} = 1000 R_{\text{Sch}}$), $\phi|_{t=0} = 0$, $\dot{r}|_{t=0} = c_R$ (or $\dot{R}|_{t=0} = V_R$), and $\dot{\phi}|_{t=0} = c_\phi$ (or $R\dot{\phi}|_{t=0} = V_\phi$). As it is seen, the trajectory of cloud varies with Γ_ϕ [compare panel (a) with (b)], Γ_R [look at panels (b) and (c)], α [panel (c): $\alpha = 0.2$ and panel (d): $\alpha = 0.1$], f [compare panel (d) with (e)], and γ [see panel (e) and (f)]. The final time, τ_f in panels (a)–(e) is equal to the time required for one round of rotation in the case of $\phi_s = 0$, but $\tau_f = 1.56$ in panel (f) is the total flight time of cloud to reach the inner boundary of ADAF, or captured radius of clumps in the case of $\phi_s = 0.004$.

variation of ϕ_s, the most change in the pattern of spiral motion happens for curves with different α, because we see a green dotted curve (with $\alpha = 0.2$) in panel (a) overlaps with a red dot–dashed one (with $\alpha = 0.2$), whereas in panel (b) and (c) when ϕ_s is not zero, these two curves remarkably different from each other. Moreover, the panels of this figure declare that time-averaged rotational velocity $(r\bar{\phi}')$ of BLR clumps is greater with larger values of Γ_ϕ, f, and γ, but smaller Γ_R and α. Similar behaviour can be deduced for the time-averaged radial velocity, i.e. $\bar{r}'$, too (except for the cases with different α's without thermal conduction as we mentioned before).

It can be interesting to know about the treatment of velocity components of BLR clouds during their flight time and compare it with the pattern of the velocity field of clumps in the first part of this paper. On the other hand, the estimation of BLR's velocity is vital for calculating emission-line width full width at half-maximum (FWHM), thus we have presented the instantaneous velocity of our typical cold cloud in Figs 9, 10, and 11. Each panel of these three figures is corresponding to one in Fig. 7. We have also added the

velocity components of ADAF (marked by red colour) to these panels and also the Keplerian velocity (blue) in Fig. 11. Notice that Figs 9 and 10 both illustrate the radial velocity but for two regions; outer part, $100 < R/R_{\text{Sch}} < 1000$ in Fig. 9 and the inner part, $10 < R/R_{\text{Sch}} < 100$ in Fig. 10. The solutions in the duration of $0 \le \tau \le 2.5$ are specified by black colour, and beyond this time are drawn by blue colour in Figs 9 and 10 (see Table 1 for the total flight time of each case). As clearly seen, these figures are very different from those in Figs 5 and 6, unlike clumps in steady-state condition, here clouds can have a positive radial velocity in some parts of their eventual path towards the centre (ref. Figs 9c–f and 10f). In the absence of the drag force, the orbital motion of clouds would be Keplerian, and they could passes a point many times, but here they cross a point up to twice (and three times in the case of panel f), but not with the same velocity or even with the same direction (look at panels c–f of Fig. 9). Comparing red and black curves (of Fig. 9) implies that the radial velocity of clouds at outer part may grow about one order of magnitude larger than ADAFs in the middle of their path, but their rotation does not show this much difference
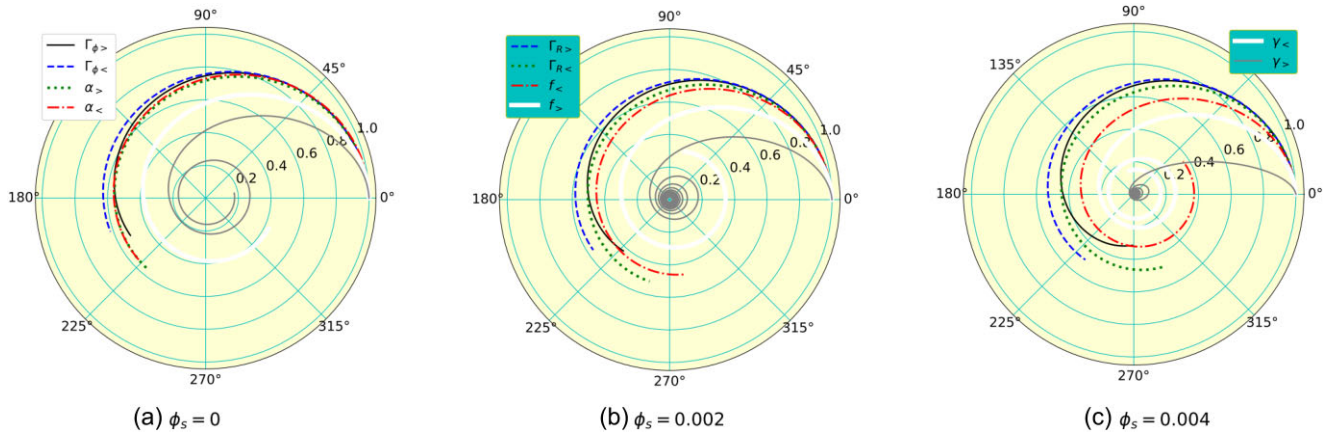
(a) $\phi_s = 0$ **(b)** $\phi_s = 0.002$ **(c)** $\phi_s = 0.004$

Figure 8. Spiral motion of a BLR cloud in the non-static medium like an ADAF. The input parameters of this figure are similar to Fig. 7, but we have selected $\tau_f = 2.5$ for all curves except for that one in panel (c) with grey colour ($\tau_f = 1.56$). In each panel, we have used: (1) black solid line for orbital motion by applying the same parameters as Fig. 7(a), (2) blue dashed line → Fig. 7(b), (3) green dotted line → Fig. 7(c), (4) red dot–dashed line → Fig. 7(d), (5) white line → Fig. 7(e), (6) grey line → Fig. 7(f). Therefore, (1) black curves have larger Γ_ϕ, comparing with blue dashed ones, (2) green dotted lines have smaller Γ_R in comparison with blue ones, but it has larger α relative to red dot–dashed curves ($\alpha = 0.1$), and (3) finally white curves have larger f comparing with red ones, but smaller γ if we compare them with grey curves ($\gamma = 1.5$).
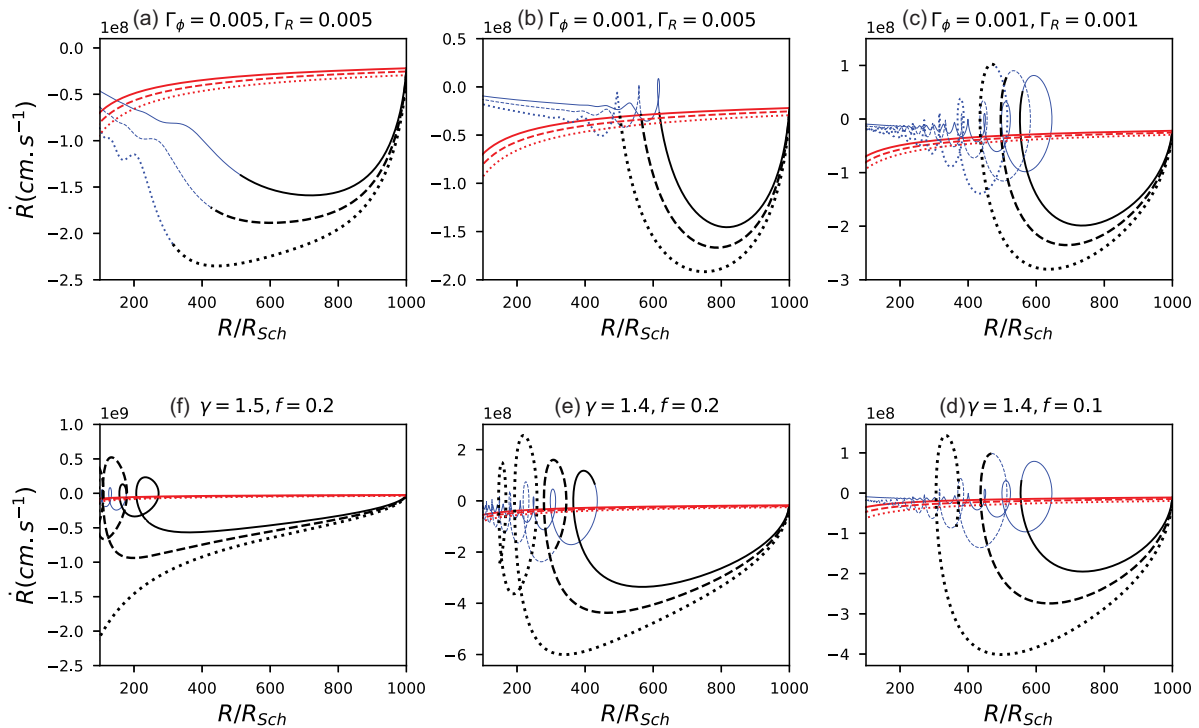

Figure 9. Time-dependent variation of the radial velocity of a BLR cloud with respect to radius. Input parameters of each panel are the same as the ones in Fig. 7, so comparing every pair of adjacent subplots yields information about the effect of a certain parameter other than ϕ_s. In each panel, the solid dashed and dotted lines refer to solutions with $\phi_s = 0, 0.002, 0.004$, respectively. Two colours have been used in this figure; the black curves represent $\dot{R}$ and the red ones show V_R of the ADAF.

(according to Fig. 11). Very different behaviour of radial velocity is seen in Fig. 10 (exception for the case of panels e, f), here there are not that many fluctuations in the magnitude of $\dot{R}$ that was in outer part. Moreover, clouds pass much more slowly in the inner part of a hot background medium with $\gamma = 1.4$ and $f = 0.1$. The small plots inside the main large plots of Fig. 11 display the angular momentum of clouds with respect to the radius (red colour curves show the ADAF's angular momentum). According to these curves,

we can see like each element of hot gas, the angular momentum of individual clumps decreases towards the centre, thus they can participate in the transportation of the total angular momentum of the disc outwards and consequently cause enhancing the accretion rate effectively.

The effect of thermal conduction on the clouds' and ADAF's velocity is apparently similar as seen in Figs 9–11. Nevertheless, we should remember that time is important for clouds. For instance, if
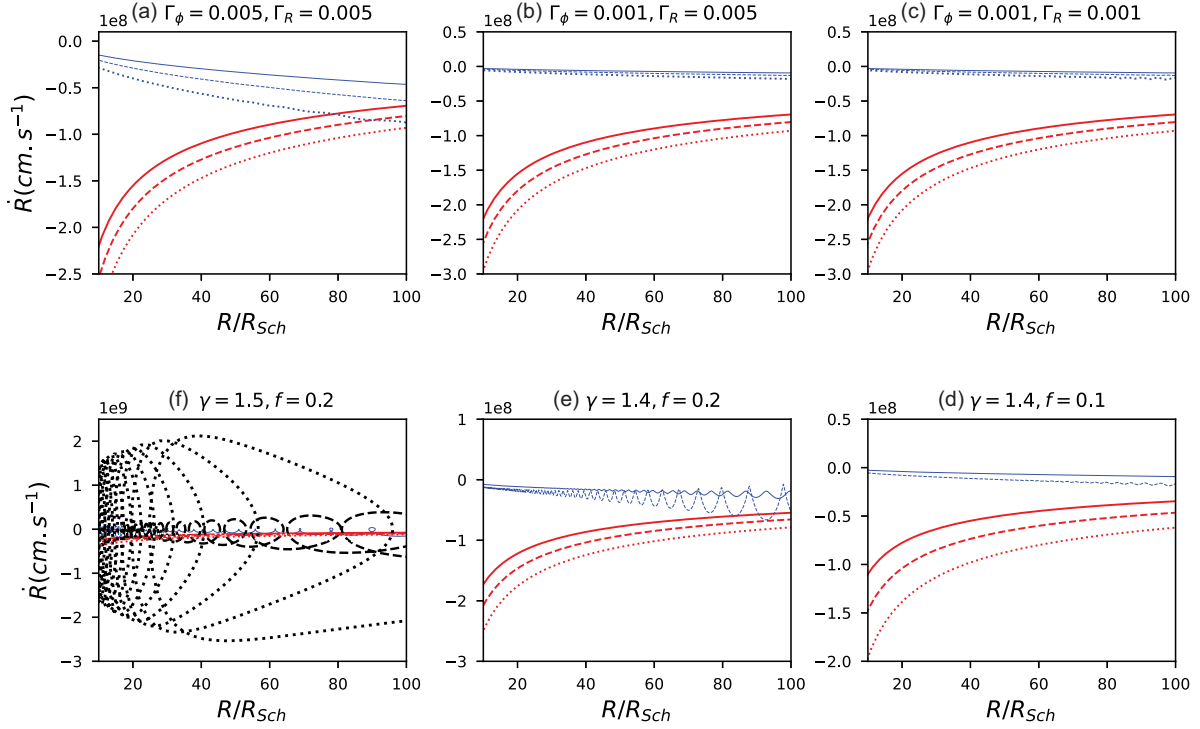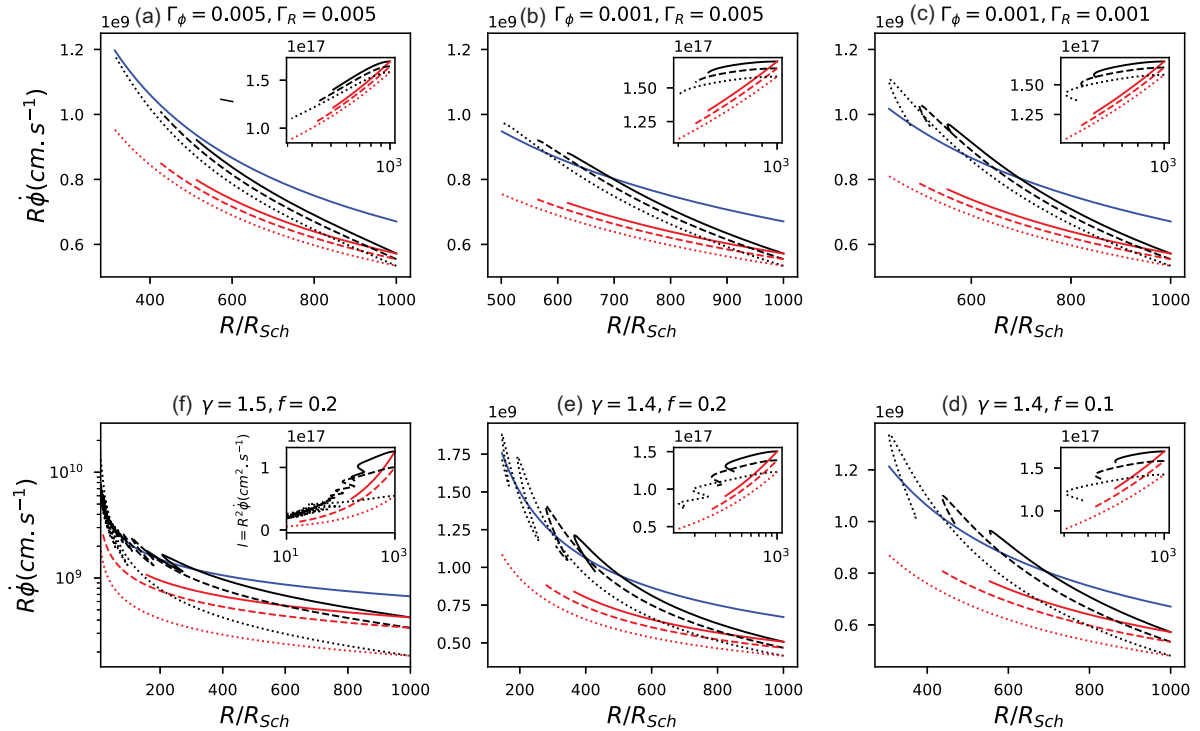
Figure 10. Time-dependent variation of the radial velocity of a BLR cloud with respect to radius. Input parameters of each panel are the same as the ones in Fig. 7, so comparing every pair of adjacent subplots yields information about the effect of a certain parameter other than ϕ_s. In each panel, the solid dashed and dotted lines refer to solutions with $\phi_s = 0$, 0.002, 0.004, respectively. Two colours have been used in this figure; the black curves represent $\dot{R}$ and the red ones show V_R of the ADAF.

Figure 11. Time-dependent variation of the rotational velocity of a BLR cloud with respect to radius. In each panel, the solid dashed and dotted lines refer to solutions with $\phi_s = 0$, 0.002, 0.004, respectively. Similar to Fig. 8, the black curves represent $R\dot{\phi}$ and the red ones show V_ϕ of the ADAF. The set of input parameters is common to the ones in Figs 7 and 8, thus we can find out the role of each parameter by comparing two related adjacent subplots. In this figure, we have also drawn plots of the angular momentum of both clumps (black curves) and ADAF (red curves) inside the main larger plots. The same line style has been used for different values of ϕ_s in smaller plots too.

Table 1. The dimensionless total flight time (τ_T) of a BLR cloud with: $\Gamma_{R,\phi} = 0.001, 0.005, f = 0.1, 0.2, \alpha = 0.1, 0.2, \gamma = 1.4, 1.5$.

ϕ_s	0	0.002	0.004
$\tau_T (\Gamma_{\phi >})$	8.41	6.41	4.95
$\tau_T (\Gamma_{\phi <}, \Gamma_{R >})$	35.33	25.11	17.77
$\tau_T (\Gamma_{R <}, \alpha_{>})$	35.05	24.86	17.52
$\tau_T (\alpha_{<}, f_{<})$	35.28	17.69	8.73
$\tau_T (f_{>}, \gamma_{<})$	11.99	7.56	4.73
$\tau_T (\gamma_{>})$	5.11	2.872	1.565

we choose a certain time, and at that time, we compare the rotational velocity of two clouds embedded in mediums with different ϕ_s and crossing two points (with different spatial coordinates), one with larger ϕ_s has a larger $R\dot\phi$ (look at Fig. 11, compare the inner last point of each curve with that of other curves); this point can be understood better by looking at Fig. 12. In Fig. 12, we have shown the variation of the two components of velocity with respect to the flight time of clumps with applying the same sets of input parameters as Fig. 8. Here again we can see how the presence of thermal conduction changes the other parameters effect on the velocity of BLR clouds during a certain time.

In Fig. 13, we have calculated the total flight time (τ_T) of a BLR cloud as a function of the thermal conduction parameter, ϕ_s. The time-scale of this figure has been evaluated by assuming $r_0 = 1000R_{Sch} \approx 0.01$ pc, $M = 10^8\,M_\odot$: $t_0 \approx 4.42 \times 10^7$ s, which is about 511.5 d or 1.4 yr. Black colour curves refer to clumps in different mediums, and also red curves show the total time needed for an element of gas

moves between outer and inner boundaries of ADAF, i.e.

$$T_A = -\int_{R_{in}}^{R_{out}} \frac{dR}{V_R} = \frac{2}{3c_R} \left[1 - \left(\frac{R_{in}}{R_{out}} \right)^{3/2} \right] t_0,$$

where $t_0 = \sqrt{R_{out}^3/GM}$. In panel (a), we have plotted the total flight time for four different sets of Γ_ϕ, Γ_R, and α with fixed values for γ (= 1.4) and f (= 0.1). As we know with larger Γ_R and Γ_ϕ clumps experience stronger drag force, but evidently the same variation in their magnitude cause different change in τ_T; apparently in dynamics of BLRs, Γ_ϕ acts more effective than Γ_R (look at Fig. 14). Regarding the role of ϕ_s in the stability of clumpy BLR systems, we see in both panels of Fig. 13, increasing ϕ_s has a negative effect on τ_T and makes it shorter. On the other hand, decreasing f and γ result shorter lifetime for clouds. Now, if we compare red curves with black ones, we can find out those clumps with smaller Γ_ϕ (black dashed and dotted curves in panel a) can be as stable as or even more stable than their host medium (or background ADAF).

In order to clarify the role of each component of drag force separately in Fig. 14, we have drawn the projection of a typical BLR cloud for three different cases: a drag force (1) with two zero components, $\Gamma_R = \Gamma_\phi = 0$ (black dot–dashed line), (2) with one zero component at the azimuthal direction, $\Gamma_\phi = 0$, and (3) with one zero component at the radial direction, $\Gamma_R = 0$. As we expect the first curve without drag force illustrates a Kepler orbit with an elliptic shape. On the other hand, although the second curve is at first elliptical, after a few moments, it converts to spherical under the influence of drag force in the radial direction, thus it becomes as stable as the first case. In contrast with first and second cases, the motion of the clump deviates significantly from
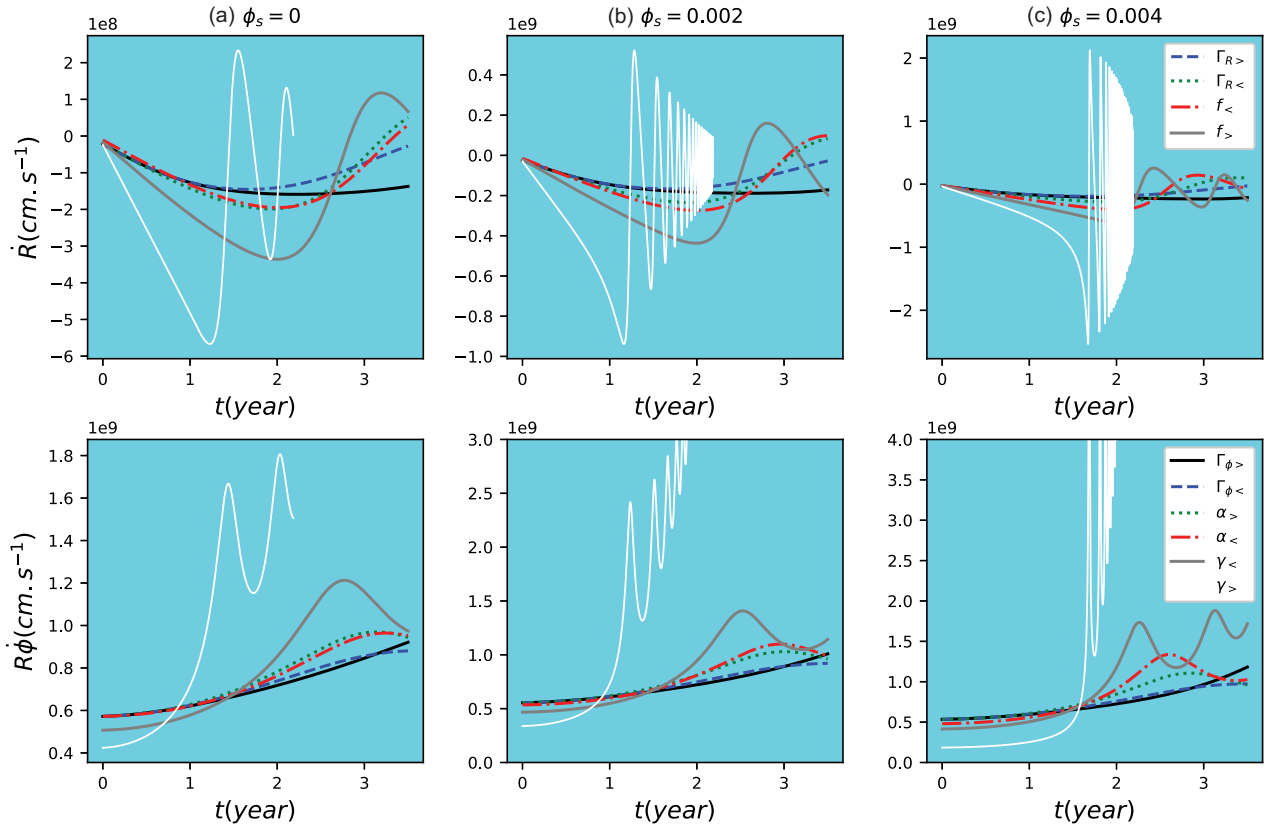

Figure 12. Variation of velocity components of a BLR cloud with respect to the flight time. The setting of input parameters is the same as in Fig. 8.
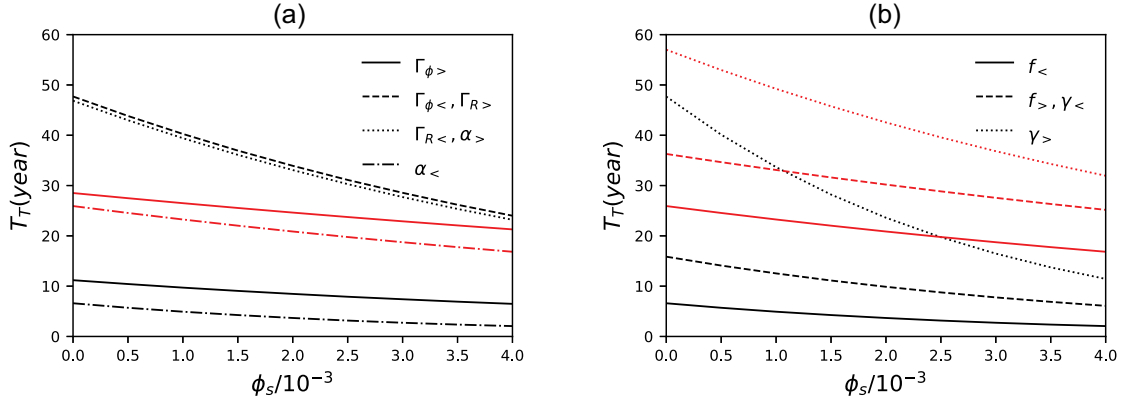
Figure 13. The total flight time of a typical BLR cloud as a function of the thermal conduction parameter with a different set of other input parameters. In panel (a), we have examined two different values of the azimutial coefficient of drag force: $\Gamma_\phi = 0.005$ (solid line, labeled by $\Gamma_{\phi>}$), $\Gamma_\phi = 0.001$ (dashed line, $\Gamma_{\phi<}$), both presented in black colour and other parameters are the same as panels (a) and (b) of Fig. 7. The other curves in panels (a) and (b) here have been drawn to study the effect of: (1) Γ_R by trying $\Gamma_{R>} = 0.005$, (presented by dashed line in panel a, other parameters are the same as Fig. 7b); $\Gamma_{R<} = 0.001$ (dotted line in panel a, others equal to ones in Fig. 7c); (2) α with choosing $\alpha_> = 0.2$ (dotted) and $\alpha_> = 0.1$ (dot–dashed; others like Fig. 7d); (3) f with two values of $f_< = 0.1$ (solid line in panel b; others like Fig. 7d) and $f_> = 0.2$ (dashed line in panel b; others like Fig. 7e); (4) γ with trying $\gamma_< = 1.4$ (dashed) and $\gamma_> = 1.5$ (dotted line in panel b; other parameters are the same as Fig. 7f). In this figure, the curves in red colour represent the total dimensionless time required for an element in ADAF reach the inner boundary (i.e. $10R_{Sch}$) from the outer boundary ($1000R_{Sch}$). In panel (a), for all values of Γ_R and Γ_ϕ, V_R does not change, hence just red solid line is corresponding to all three set of input parameters: ($\Gamma_\phi = \Gamma_R = 0.005$), ($\Gamma_\phi = 0.001$, $\Gamma_R = 0.005$), and ($\Gamma_\phi = \Gamma_R = 0.001$).
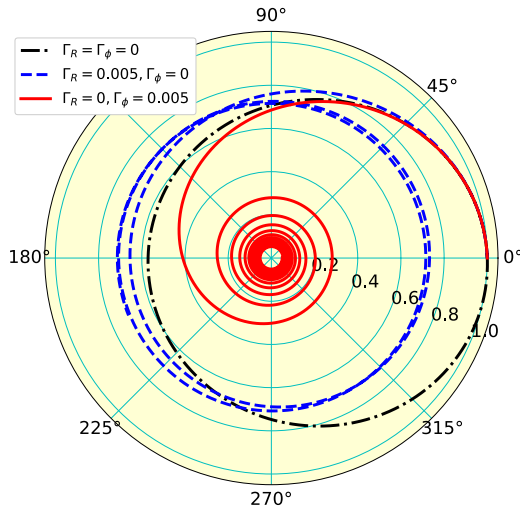

Figure 14. The trajectory of a BLR cloud with three different drag forces. The black dot–dashed line corresponds to $\Gamma_R = \Gamma_\phi = 0$, the blue dashed line is related to $\Gamma_R = 0.005$, $\Gamma_\phi = 0$, and red solid line is evaluated by choosing $\Gamma_R = 0$, $\Gamma_\phi = 0.005$. The other parameters are: $\alpha = 0.2$, $f = 0.1$, and $\gamma = 1.4$. The used fight times in this figure are $\tau_f = 5$, 10, and 5.5 for the cases with $\Gamma_{R,\phi} = 0$, $\Gamma_\phi = 0$, and $\Gamma_R = 0$, respectively.

Keplerian in the light of a drag force with a single component in ϕ direction.

6 SUMMARY AND CONCLUSION

In this paper, we investigated the effect of thermal conduction on the dynamics of cold clouds (or clumps) embedded in a hot accretion flow (ADAF) which experiences a drag force. We took two different approaches to this problem: first, we supposed the clouds behave like collision-less particles and move with a velocity vector whose averaged value equals their host medium velocity, and secondly, we concentrated on clouds individually to find the position

and instantaneous velocity of a typical cloud. In all parts of this study, we presumed axisymmetric and steady-state configuration for the background medium of clumps as long as we supposed that all particles have negligible vertical motions. The effect of thermal conduction appeared in this problem due to involving drag force between clouds and ADAF. We employed ADAF solutions including thermal conduction presented by Tanaka & Menou (2006). For the first part, we followed Wang et al. (2012) and applied Boltzmann equations in order to obtain the root mean velocity square of the clumps (or two components of velocity dispersion), i.e. $\langle v_R^2 \rangle^{1/2}$ and $\langle v_\phi^2 \rangle^{1/2}$. The value of $\langle v_R^2 \rangle^{1/2}$ is important since the capture rate of the clumps at the inner edge of the disc is directly proportional to the ratio of $\langle v_R^2 \rangle^{1/2} / \langle v_R \rangle$ (ref. equation 34 of WCL12). We should mention that our results were a bit different even in the absence of thermal conduction with ones presented by WCL12, because of the opposite direction of our drag force; we ratiocinated that after applying the approximation of equal average velocity with ADAF's one, an average value of drag force must remain at the same sign as majority particles drag force sign (in the opposite direction of their relative velocity with ADAF). This tiny change in the drag force formula led to clumps with $\langle v_\phi^2 \rangle^{1/2}$ smaller than the rotational velocity of ADAF that was evaluated as larger in the previous work. Furthermore, our adopted drag force had an effect on a critical (or minimum) value for the drag force coefficient in the azimuthal direction instead of the radial direction in WCL12.

For the second part, we found the trajectory of a single clump in the same way as a classical two-body problem. The similar results for the influence of thermal conduction were achieved from both parts; when we added a larger permissible (ref. Fig. 4) value for the thermal conduction parameter, ϕ_s, the solutions changed to reduce velocity in the azimuthal direction but growing it in the radial direction. However, we found out the function of rotational velocity of a cloud behaves in opposite way with time; it may become larger with a greater ϕ_s (ref. Fig. 12). Furthermore, we compared the total flight time (needed a clump to move from outer region of ADAF to the capture radius) of BLR clouds with the total dynamical time of a

volume element of ADAF. We faced to this point: if clouds move with a very small or even zero friction in the azimuthal direction, they can survive from the central captured region of ADAF. On the other hand, we saw the existence of a little friction along ϕ-direction modifies a Kepler orbit of clumps to a spiral one and can make it a short-lived object. The similar works had been done by Shadmehri (2015, who studied clouds in a laminar flow) and Khajenabi (2016; who worked on BLRs in a turbulent flow); both considered drag force and also repulsive radiation force from the central object. For simplicity and having the similar condition as the first part of our work, we did not take into account radiation force on this problem and assumed clumps moved at the equatorial plane under the influence of central gravity and drag force. We found out how much the stability of a BLR system can be changed by characteristic parameters (that is, α, f, and γ) of their hot host medium.

To improve this work, it is good for both parts to write equations in spherical coordinates and apply 2D $(r - \theta)$ solutions of ADAFs, which included v_θ and let us study the vertical motion of clumps too. For little improvement, we can use a formula composed of both linear and quadratic relative velocity (between the clumps and the gas) with two optional coefficients (0, 1) set by the Reynolds number.

ACKNOWLEDGEMENTS

DATA AVAILABILITY

No new data were generated or analysed in support of this research

REFERENCES

Abbassi S., Ghanbari J., Ghasemnezhad M., 2010, MNRAS, 409, 1113
Abbassi S., Ghanbari J., Najjar S., 2008, MNRAS, 388, 663
Blaes O., Socrates A., 2001, ApJ, 553, 987
Blaes O., Socrates A., 2003, ApJ, 596, 509
Bu D.-F., Gan Z.-M., 2018, MNRAS, 474, 1206
Burkert A., Schartmann M., Alig C., Gillessen S., Genzel R., Fritz T. K., Eisenhauer F., 2012, ApJ, 750, 58
Celotti A., Rees M. J., 1999, MNRAS, 305, L41
Cowie L., McKee C. 1977, ApJ, 211, 146
Das U., Sharma P., 2013, MNRAS, 435, 2431
Frank J., King A., Raine D., 1992, Accretion Power in Astrophysics, 2nd edn. Cambridge Univ. Press, Cambridge
Fromerth M. J., Melia F., 2001, ApJ, 549, 205
Gammie C., 1998, MNRAS, 297, 929
Ghasemnezhad M., Khajavi M., Abbassi S., 2012, ApJ, 750, 57
Ghayuri M., , 2006, MNRAS, 462, 490
Ghayuri M., 2016, MNRAS, 462, 490
Gillessen S. et al., 2012, Nature, 481, 51
Gillessen S. et al., 2013, ApJ, 763, 78
Guilbert P. W., Rees M. J., 1988, MNRAS, 233, 475
Humi M., Carter T., 2002, Celest. Mech. Dyn. Astron., 84, 245
Khajenabi F., 2015, MNRAS, 446, 1848
Khajenabi F., 2016, ApJ, 828, 9
Khajenabi F., 2016, ApJ, 828, 9
Khajenabi F., Rahmani M., Abbassi S., 2014, MNRAS, 439, 2468
Krause M., Burkert A., Schartmann M., 2011, MNRAS, 411, 550
Krause M., Schartmann M., Burkert A., 2012, MNRAS, 425, 3172
Krolik J. H., 1988, ApJ, 325, 148
Krolik J. H., McKee C. F., Tarter C. B., 1981, ApJ, 249, 422
Krolik J., 1998, ApJ, 498, L13
Kumar P., 1999, ApJ, 519, 599
Kuncic Z., Blackman E. G., Rees M. J., 1996, MNRAS, 283, 1322
Landau L. D., Lifshitz E. M., 1959, Fluid Mechanics. Pergamon, Oxford
Malzac J., Celotti A., 2002, MNRAS, 335, 23
Marconi A., Axon D. J., Maiolino R., Nagao T., Pastorini G., Pietrini P., Robinson A., Torricelli G., 2008, ApJ, 678, 693
Mavraganis A. G., Michalakis D. G., 1994, Celest. Mech. Dyn. Astron., 58, 393
Merloni A., Malzac J., Fabian A. C., Ross R. R., 2006, MNRAS, 370, 1699
Mittleman D., Jezewski D., 1982, Celest. Mech., 28, 401
Namekata D., Umemura M., Hasegawa K., 2014, MNRAS, 443, 2018
Narayan R., Mahadevan R., Quataert E., 1998, in Theory of Black HoleAccretion Disks. Cambridge Univ. Press, Cambridge, p. 148
Narayan R., Ozel F., Sironi L., 2012, ApJ, 757, L20
Narayan R., Yi I., 1994, ApJ, 428, L13
Narayan R., Yi I., 1995, ApJ, 452, 710
Netzer H., Marziani P., 2010, ApJ, 724, 318
Piran T., 1978, ApJ, 221, 652
Pittard J. M., Dyson J. E., Falle S. A. E. G., Hartquist T. W., 2003, A&A, 408, 79
Plewa P. M., Schartmann M., Burkert A., 2013, MNRAS, 431, L127
Rees M. J., 1987, MNRAS, 228, 47
Rees M. J., Begelman M. C., Blandford R. D., Phinney E. S., 1982, Nature, 295, 17
Schartmann M., Meisenheimer K., Camenzind M., Wolf S., Tristram K. R. W., Henning T., 2008, A&A, 482, 67
Shadmehri M., 2008, Ap&SS, 317, 201
Shadmehri M., 2015, MNRAS, 451, 3671
Smith J. E., Robinson A., Young S., Axon D. J., Corbett E. A., 2005, MNRAS, 359, 846
Spruit H. C., 2010, preprint (arXiv:1005.5279)
Sutherland R. S., Dopita M. A., 1993, ApJS, 88, 253
Tanaka T., Menou K., 2006, ApJ, 649, 345
Vishniac E. T., 1994, ApJ, 428, 186
Wang J.-M., Cheng C., Li Y. R., 2012, ApJ, 748, 147
Yu X.-D., Ma R.-Y., Li Y.-P., Zhang H., Fang T.-T., 2018, MNRAS, 476, 2045
Yuan F., 2003, ApJ, 594L, 99
Yuan F., Narayan R., 2014, ARA&A, 52, 529

This paper has been typeset from a TEX/LATEX file prepared by the author.